RSC Advances

PAPER

View Article Online
View Journal | View Issue

Cite this: *RSC Adv.*, 2025, **15**, 83

Impact of aspect ratio and crystal size distribution of L-glutamic acid formed by cooling crystallization on drying characteristics†

Jong Beom Lee,[a] Yu-Jin Kim,[a] Kwang-Joo Kim,[a] Geon-Hee Kim,[b] Chanmin Lee,[c] Young Duk Park,[d] Jung-Chul An,[e] Hyenoseok Yi,[e] Kyeongseok Oh[f] and Joo-Il Park *[g]

This study investigated the impact of aspect ratio and crystal size distribution on the mother liquor content and drying rate of L-glutamic acid (LGA). LGA cooling crystallization was performed using two methods: spontaneous nucleation and seeding. First, to identify various crystalline forms of LGA and obtain α-form seeds, cooling crystallization was carried out through spontaneous nucleation and seeding. Seeding improved the aspect ratio of the crystals, and both α- and β-form crystals had hexagonal shapes when their aspect ratio was enhanced. During seeding, the aspect ratio of α-form seeds improved under slow cooling rates and low supersaturation, while that of β-form seeds improved under fast cooling rates and high supersaturation. When assessing drying efficiency based on mother liquor content and drying rate, the highest efficiency was observed in crystals with an average aspect ratio of 1.25 and an average particle diameter of 416 μm, with a mother liquor content of 5.60%. Conversely, the lowest efficiency was found in crystals with an average aspect ratio of 16.40 and an average particle diameter of 170 μm, resulting in a mother liquor content of 25.21%. The time required for complete drying in these two cases showed a roughly twofold difference, taking approximately 120 minutes for the highest efficiency case and 240 minutes for the lowest. Consequently, this study was able to evaluate the drying efficiency of LGA crystals with varying aspect ratios and other crystal size distributions (CSD) in terms of mother liquor content and drying rate.

Received 16th August 2024
Accepted 27th November 2024

DOI: 10.1039/d4ra05935b

rsc.li/rsc-advances

1. Introduction

L-Glutamic acid (LGA) is one of the 20 amino acids used by cells to synthesize proteins. In addition to its role in protein synthesis, LGA is a precursor to γ-aminobutyric acid, an inhibitory neurotransmitter in the central nervous system. It is also used in the food industry, particularly in the production of monosodium L-glutamate and seasonings. LGA is a polymorph that possesses more than one crystalline form, with the known forms being the α (rhombic) and β (needle-like) forms.[1] LGA is industrially produced *via* the action of microorganisms or fermentation; however, high-purity LGA can only be obtained through further separation and purification, such as by membrane separation, electrodialysis, and crystallization.[2] During crystallization, the target substance is recovered as solid crystals from a solution. In addition to the operating conditions of the crystallization process, downstream crystal recovery and transport are important considerations for obtaining high-quality crystals. Isotropic crystals are preferred for effective downstream processing, and α-form crystals are more isotropic than β-form crystals.[3,4] Therefore, the crystallization industry may require selective crystallization to obtain isotropic crystals, such as those of the α form.

Previous studies indicate that the key process variables for obtaining α-form LGA are supersaturation, cooling rate, and temperature. Supersaturation is an important driving force in crystallization;[5] the spontaneous nucleation of α-form crystals can be observed at high supersaturation, whereas β-form crystals are observed at low supersaturation. Moreover, α-form

[a]Department of Chemical & Biological Engineering, Hanbat National University, Daejeon 34158, Republic of Korea
[b]Department of Mechanics-Materials Convergence System Engineering, Hanbat National University, Daejeon 34158, Republic of Korea
[c]Green and Sustainable Materials R&D Department, Research Institute of Clean Manufacturing System, Korea Institute of Industrial Technology, 89 Yangdaegiro-gil, Ipjang-myeon, Cheonan-si 31056, Republic of Korea
[d]Innovation Corporation for Smart Optics, Hanbat National University, Daejeon 34014, Republic of Korea
[e]Carbon Materials Research Group, Research Institute of Industrial Science & Technology (RIST), Pohang 11 37673, Republic of Korea
[f]Department of Chemical & Biological Engineering, Inha Technical College, Incheon 22212, Republic of Korea
[g]Department of Chemical & Biological Engineering, Hanbat National University, Daejeon 34158, Republic of Korea. E-mail: jipark94@hanbat.ac.kr; Tel: +82 42 8211530

† Electronic supplementary information (ESI) available. See DOI: https://doi.org/10.1039/d4ra05935b

crystals are preferentially obtained at low temperatures.[6,7] Existing studies focus on the selective preparation of specific crystalline forms of LGA, particularly the α and β forms. Zhenguo *et al.* reported that using a batch crystallizer allows for the precise control of polymorphs during cooling crystallization.[8] Ma *et al.* reported that continuous crystallization using mixed-suspension mixed-product-removal crystallizers is feasible for polymorphs such as LGA.[9] Ni *et al.* reported that using an oscillatory baffled crystallizer (OBC) can reduce the induction time for nucleation.[10] Other studies have also shown that using an OBC allows for precise control over continuous processes and crystallization.[11,12] Recent studies have aimed to precisely control polymorphs in real time using analytical techniques such as Fourier transform infrared and Raman spectroscopy.[13–16] These methods can determine the optimal conditions for controlling the polymorphism of LGA and are effective in identifying the fraction of each crystalline form or transformation conditions at a specific supersaturation level or temperature. However, in some cases, the nucleation of β-form crystals occurs on the surface of α-form crystals, rendering polymorphism control difficult.[15,17–19] Lindenberg *et al.* and Liang *et al.* attempted to solve these issues through simulations.[20,21] Simulations with thermodynamic and kinetic data can be used to achieve precise process control. During crystallization, polymorphism tends to favor thermodynamically stable and kinetically metastable forms.[22,23] The α form is thermodynamically metastable, while the β form is stable. Tahri reported that the prolonged agitation of metastable α-form crystals can lead to their transformation into stable β-form crystals.[24] Sakata reported measuring the velocity of the α-β transition in the dry state by heating α-crystals in a hot air bath.[25]

Crystals with large aspect ratios can cause filter blinding during filtration.[5,26,27] Reducing the aspect ratio of the crystals can minimize this issue. Seeding is a common method used to alter the shape of a crystal by reducing unnecessary nucleation and promoting seed growth.[28] Unlike spontaneous nucleation, this process involves only crystal growth,[29,30] and the shape of the growing crystals can vary depending on the crystal habit. Seeding enables better control of the crystal size distribution (CSD),[31,32] higher yields, and reduced process times. Dhanasekaran *et al.* reported that LGA crystals grow into a hexagonal shape after seeding.[33] This study found that using α-form seeds resulted in increased isotropic crystal growth. By contrast, Zhang *et al.* investigated changes in crystal shape using β-form seeds with a large aspect ratio,[34] Liu *et al.* investigated crystal growth kinetics and CSD using β-form seeds.[35] Most studies focus on selective crystallization and changes in crystalline form, specifically between the α and β forms, through seeding. However, limited research on the differences between the two crystalline forms in downstream processes, such as precipitation, filtration, drying, and transportation, is available. Therefore, further investigation of the differences in these processes depending on the crystalline forms of LGA, as well as methods to improve their aspect ratio, is necessary. Given this background, this study aimed to investigate the differences in the downstream processes of different crystalline forms of LGA. Specifically, cooling crystallization was performed using a batch reactor, and LGA crystals were obtained through spontaneous nucleation and seeding. Seeds of the α (rhombic) and β (columnar) forms were used. The mother liquor content and drying rate of the produced crystals were measured and compared to investigate the effect of their aspect ratio on their filtration and drying processes.

2. Experimental

2.1 Materials and experimental equipment

Powdered LGA (F.W. 147.13, assay min 99.0%; DUKSAN, Korea, Fig. 1) and distilled water were used to prepare the LGA solution. Mass was measured using scales (GR-200, A&D; Adventurer AR5120, OHAUS). A 200 mL double-jacketed glass vessel and stirrer (HS-100D, DAIHAN Scientific) equipped with a triple-blade impeller were used to mix the powder and distilled water. The stirring rate is constant at 300 rpm. A circulator (RW-2025G, JeioTech) connected to the double-jacketed vessel was used to control the temperature of the LGA solution. The solution containing the generated crystals was filtered through an aspirator (VE-11, JeioTech) and glass filter (17G4, PYREX). Optical microscopy (OM, JP CX-31, OLYMPUS) was used to inspect the shape of the crystals produced in the experiment, and their crystalline form was confirmed using X-ray diffraction (XRD) analysis (SmartLab, Rigaku). In this study, each experimental case was numbered and referred to as a 'Run'.

2.2 Crystallization process

2.2.1 Cooling crystallization method. The LGA solution was allowed to reach equilibrium and then cooled to the target temperature to induce crystal generation. Cooling can be performed by decreasing the temperature uniformly over time or rapidly in an exponential curve.[32,36] LGA crystals can be obtained

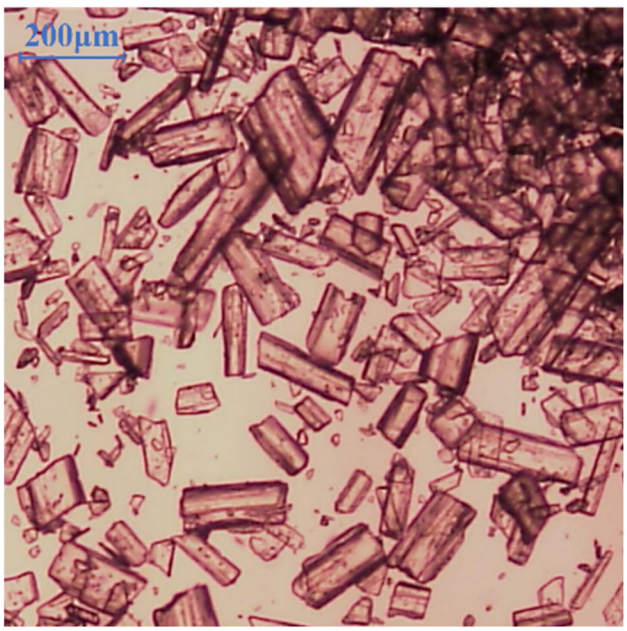

Fig. 1 Optical micrographs (OM) of β-form LGA.

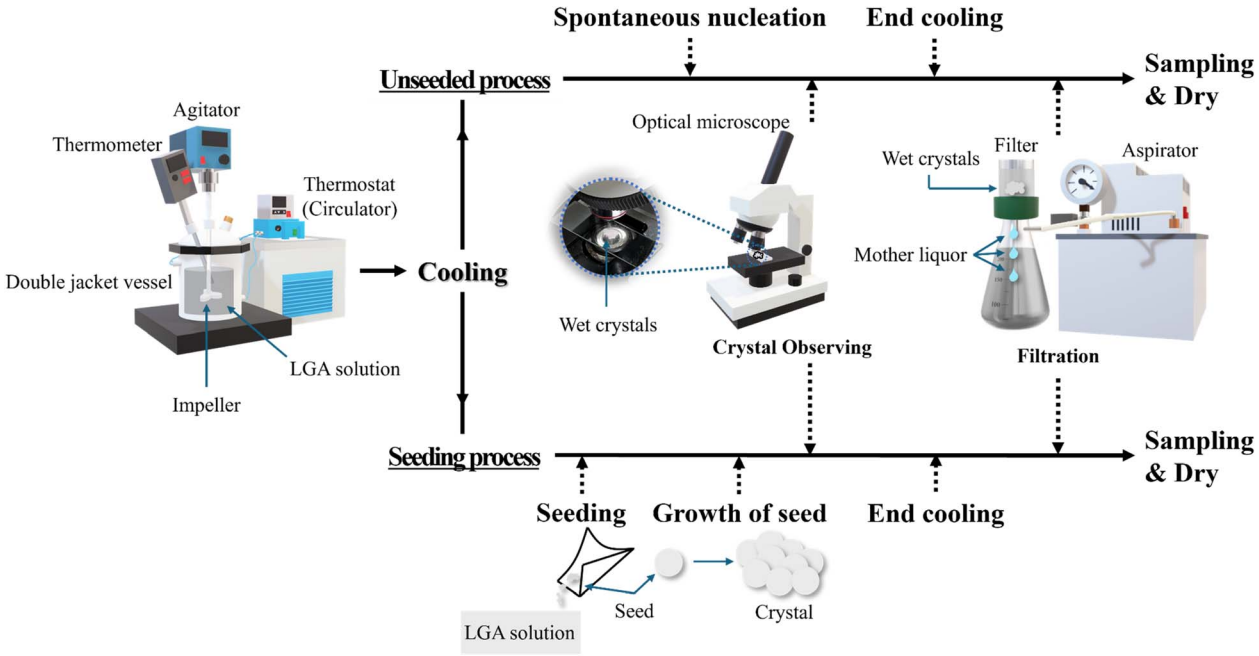

Fig. 2 Schematic illustration of the experiment process: unseeded (spontaneous nucleation) and seeding crystallization process.

via spontaneous nucleation or seeding. When the solution reached the final temperature, it was maintained for 1 h, and the generated crystals were sampled and observed under an optical microscope. The LGA solution containing the crystals was filtered to remove the mother liquor. The crystals remaining on the filter were collected, and their masses were measured at regular intervals to analyze their drying characteristics. Fig. 2 present the experiment process in this study.

2.2.2 Solubility. The solubility of the LGA solution was measured at its equilibrium point (Fig. 3). Approximately 100 g of the solvent (distilled water) was mixed with a specific mass of LGA in a double-jacketed vessel. If equilibrium was reached, more solute was added to the mixture; otherwise, the temperature was increased at a rate of 0.167 K min^{-1}. The solutions were maintained at each temperature for 3 h to ensure accurate solubility measurements. This process was repeated to determine the equilibrium points of all solutions. The temperature range for the solubility measurements in this study was 283–343 K, and the temperature was increased at 10 K intervals. The supersaturation values at specific temperatures were calculated from the solubility data shown in Fig. 3 and are presented in Table 1. Eqn (1) is a regression line calculated using the least squares method from a log plot of the solubility data ($R^2 = 0.9992$). Eqn (1) was used to calculate the saturation mole fraction of the solute at any given temperature, which, in turn, allowed for the calculation of the saturation concentration. Eqn (2) was used to numerically represent supersaturation in this study; in this equation, C and C_{sat} are the initial and saturation concentrations of the LGA solution, respectively.

$$\ln(X_{Solute}) = 11.5344 \ln(T) - 72.7282 \quad (1)$$

$$\sigma = \frac{C - C_{sat}}{C_{sat}} \quad (2)$$

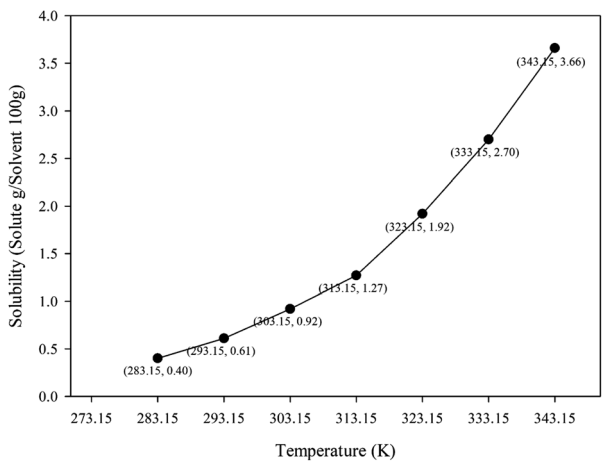

Fig. 3 Solubility of β-form LGA.

Table 1 Molar fraction and temperature log–log plot of β-LGA solution

T (K)	Solubility (g/100 g)	X_{Solute}	ln (T)	ln (X_{Solute})
283	0.40	0.0004891238	5.6460	−7.6229
293	0.61	0.0007457223	5.6807	−7.2012
303	0.92	0.0011242698	5.7142	−6.7906
313	1.27	0.0015513177	5.7467	−6.4687
323	1.92	0.0023434385	5.7781	−6.0561
333	2.70	0.0032923260	5.8086	−5.7162
343	3.66	0.0044577126	5.8382	−5.4131

2.2.3 Metastable zone limit. The temperature at which spontaneous nucleation occurred was identified to determine the metastable zone limit.[37–39] The interval between the temperatures at which the saturation concentration and spontaneous nucleation occur corresponds to the metastable zone width (MSZW). In this study, MSZW was measured by excluding cases in which spontaneous nucleation occurred at excessively high or low temperatures, considering that the solvent was water (ESI 1†). The solution was prepared by adding 2.4 g, 2.7 g, 3.0 g, and 3.3 g of solute to 100 g of solvent (distilled water), respectively.

3. Result and discussion

3.1 Unseeded (spontaneous) nucleation

Based on the crystalline form and supersaturation levels observed at various cooling rates, it was found that faster cooling rates and higher supersaturation levels promote the formation of α-form LGA (ESI 2 and 3†). Because supersaturation is driven by temperature differences, a high level of supersaturation indicates a large temperature difference owing to cooling. These results are consistent with previous studies that found that the α form is preferentially formed at lower temperatures.[6,7] Faster cooling rates tended to favor the predominant generation of α-form crystals because this form produces stable hydrogen bonds at low temperatures; differences in the positions of crystal growth may also influence the crystal form.[36] Additionally, the differences in crystal shape may be attributed to the crystal habit, which dictates how the crystals grow after nucleation.[40] Thus, fast cooling rates may be inferred to be required to obtain α-form crystals through spontaneous nucleation.

In this study, switching between two circulators was utilized to rapidly cool the LGA solution. Here, the solution was transferred from a high-temperature (343 K) circulator to a low-temperature (283 K) circulator connected to the double-jacketed vessel, resulting in a rapid cooling effect that caused the temperature to decrease exponentially rather than linearly (ESI 4†). Switching did not induce cooling at a fixed cooling rate, such as 1 K min^{-1}, but rapidly decreased the temperature at the beginning of the cooling process. Thus, α-form crystals were successfully obtained through spontaneous nucleation,[7] as shown in Fig. 4.

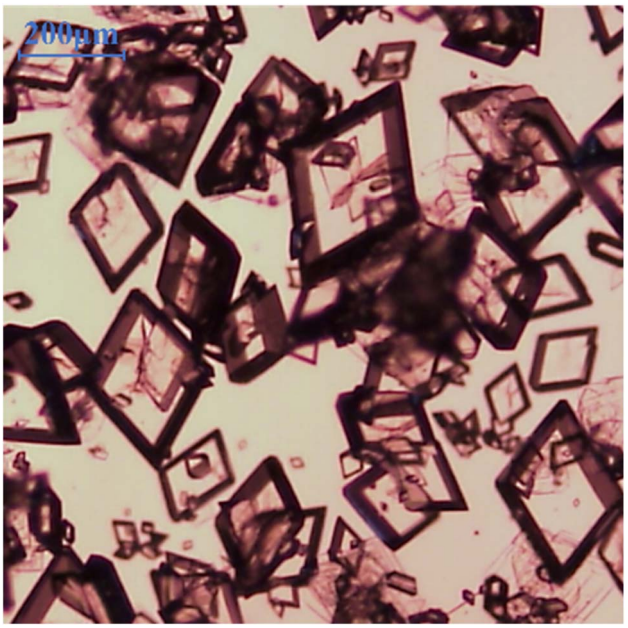

Fig. 4 Image of α-form LGA by switch method.

3.2 Seeding

Two types of seeds were used: the β-form seed shown in Fig. 1 and the α-form seed shown in Fig. 4. The crystals grown used β-form seed are shown in Fig. 5 and the crystals grown used α-form seed are shown in Fig. 6. The conditions used for the seeding experiments are listed in Table 2. Supersaturation was calculated from the seeding temperature, and the supersaturation of Table 2 was calculated and represented along with the initial concentration. In all seeding experiments, the solution was prepared with an initial concentration of 2.7 g of solute per 100 g of distilled water.

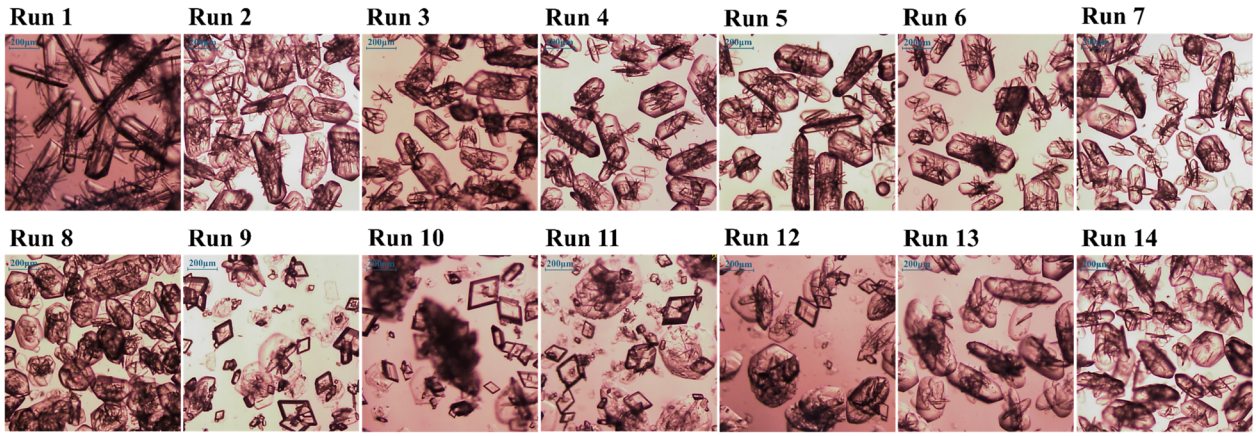

Fig. 5 OM image of LGA crystals using β-form seed in Table 2: Run 1 to Run 4 have different cooling rate, Run 5 to Run 8 have different supersaturation and Run 9 to Run 14 are about the effects of seed mass.

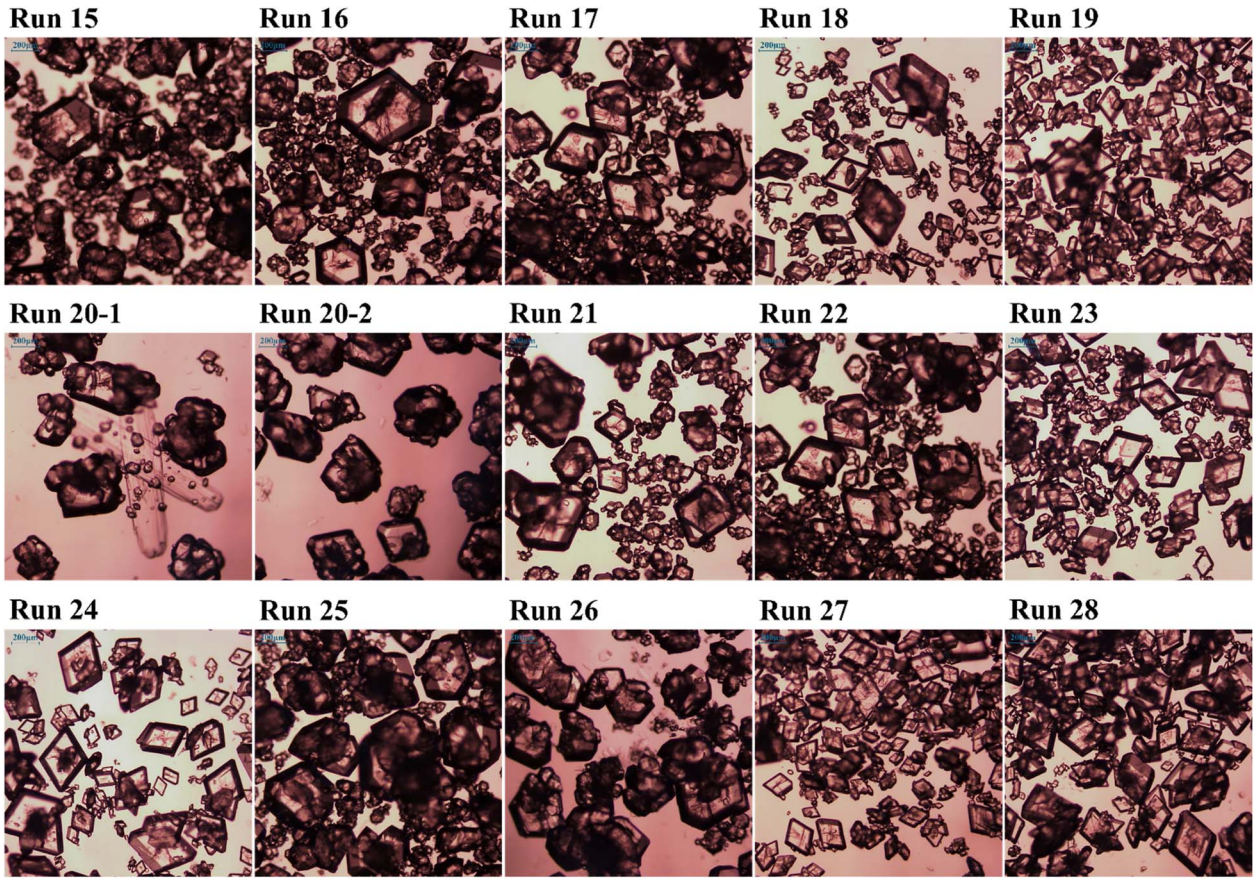

Fig. 6 OM image of LGA crystals using α-form seed in Table 2: Run 15 to Run 19 have different cooling rate, Run 20 to Run 24 have different supersaturation and Run 24 to Run 28 are about the effects of seed mass.

Runs 1–4 were conducted at a cooling rate of 0.4 K min^{-1}, which was the highest cooling rate at which the spontaneous nucleation of α-form seeds did not occur. An increase in supersaturation tended to decrease the aspect ratio of the crystals formed from β-form seeds. Seeding at temperatures below 288 K to achieve higher supersaturation may be expected to further improve the aspect ratio. However, this approach brings the process closer to the metastable zone limit, which may lead to spontaneous nucleation. For Runs 5–8, the aspect ratio of the formed crystals decreased as the cooling rate increased at the same level of supersaturation. In the case of rapid cooling (Runs 9 and 10), α-form crystals were observed, indicating that the β-form seeds did not grow sufficiently. This phenomenon may be attributed to the fact that the seed mass was only approximately 1% of the solute mass, which is too low for sufficient crystal growth. If the seed mass is sufficient, unnecessary nucleation may be avoided (Runs 13 and 14).

At a cooling rate of 0.6 K min^{-1}, which was the cooling rate at which the spontaneous nucleation of β-form seeds did not occur, the α-form seeds grew and changed in shape from rhombic to hexagonal at low supersaturation levels. The aspect ratio decreased at low supersaturation levels (Run 15–19). These results are in contrast to those of the β-form seeds (Runs 1–4), which showed improvements in the aspect ratio of the resulting crystals under high supersaturation. In the case of Run 20, the α-form seeds grew, but the nucleation of the β-form seeds also occurred. In Runs 21–23, β-form seed nucleation was not observed, but no significant improvement in the aspect ratio of the obtained crystals was noted. Similarly, in Run 24, in which the cooling rate involved switching, no improvement in aspect ratio was observed. If the seed mass is sufficient, unwanted nucleation can be prevented, similar to the case for the β-form seeds. However, the spontaneous nucleation of the β-form seeds can still occur under a slow cooling rate.

3.3 XRD analysis

The XRD patterns for the needle-like shape, β-form seed, Run 8, α-form seed, and Run 25 are presented in Fig. 7. For α-form seed, the XRD analysis results indicated that a minor presence of the β-form was observed, but the proportion of the α-form was significantly higher. The peaks detected at $2\theta = 10°$, 30°, and 66° are characteristic of the β-form seeds, while those at $2\theta = 18.5°$, 24°, and 27° are characteristic of the α-form seeds.[41] The crystals of the powdered LGA (Fig. 1) used in the experiment are of the β form. Runs 8 and 25 confirmed that the crystalline forms of the seeds were preserved. Although the focus of seeding in this study was not transformation, the preservation of crystal form can be attributed to differences in crystal growth positions depending on the crystal habit[21] and the insufficient time for the metastable α-form crystals to transform into the β form.[24,42]

Table 2 Experiment conditions of seeding[a]

Run	Seed	Cooling rate (K min^{-1})	Seed mass (%)	$T_{Seeding}$ (°C)	$\sigma_{Seeding}$
Run 1	β-	0.4	10.0	40	1.08
Run 2	Form			30	2.03
Run 3				22	3.12
Run 4				17	4.02
Run 5	β-	0.6	10.0	17	4.02
Run 6	Form	1.0			
Run 7		1.4			
Run 8		Switch			
Run 9	β-	Switch	1.0	40	1.08
Run 10	Form			30	2.03
Run 11				17	4.02
Run 12			2.5	30	2.03
Run 13			5.0		
Run 14			10.0		
Run 15	α-	0.6	5.0	40	1.08
Run 16	Form			35	1.51
Run 17				30	2.03
Run 18				25	2.67
Run 19				17	4.02
Run 20	α-	0.2	5.0	30	2.03
Run 21	Form	0.4			
Run 22		0.6			
Run 23		0.8			
Run 24		Switch			
Run 25	α-	0.6	5.0	40	1.08
Run 26	Form		10.0		
Run 27			5.0	17	4.02
Run 28			10.0		

[a] $\ln(x_{Solute}) = 11.5344 \ln(T_{Seeding}) - 72.7282$, $\sigma_{Seeding} = \frac{C - C_{sat}}{C_{sat}}$ ($\sigma_{Seeding}$: supersaturation of spontaneous nucleation).

3.4 (Dry/wet)% and drying speed

The drying rates of four types of crystals—needle-like, Run 8, α-form seed, and Run 25 are presented in Fig. 8. Drying was conducted by collecting the crystals obtained immediately after filtration, spreading them evenly on a Petri dish, and placing it on a scale to measure weight changes at room temperature. The ambient temperature was maintained at 298 K. Weight changes were measured at time intervals of 0, 30, 60, 90, 120, 150, 180, 210, 240, 270, 300, 330, and 360 minutes. (Dry/wet)% represents the mass percentage of a dried crystal relative to its initial mass containing the mother liquor by eqn (3). Each crystal dried completely within 240 min. Among the crystals investigated, needle-like shape contained the most mother liquor, whereas those obtained in Run 25 contained the least. In addition, the crystals obtained in Run 25 dried the fastest. In the experiments using β-form seeds, the crystals obtained in Run 8 showed the greatest improvement in aspect ratio. However, the drying rates of these crystals did not differ significantly from that of the needle-like crystals. When the removal rates of the mother liquor between the fastest drying interval (after 60 min) and end of drying (after 360 min) were compared, Run 25, α-form, Run 8, and needle-like shape showed differences of approximately 0.4%, 5%, 11%, and 14%, respectively.

$$(\text{Dry/wet})\% = \frac{\text{mass of dried crystal at a specific time (g)}}{\text{initial mass of crystal with 100\% mother liquor (g)}} \times 100(\%) \quad (3)$$

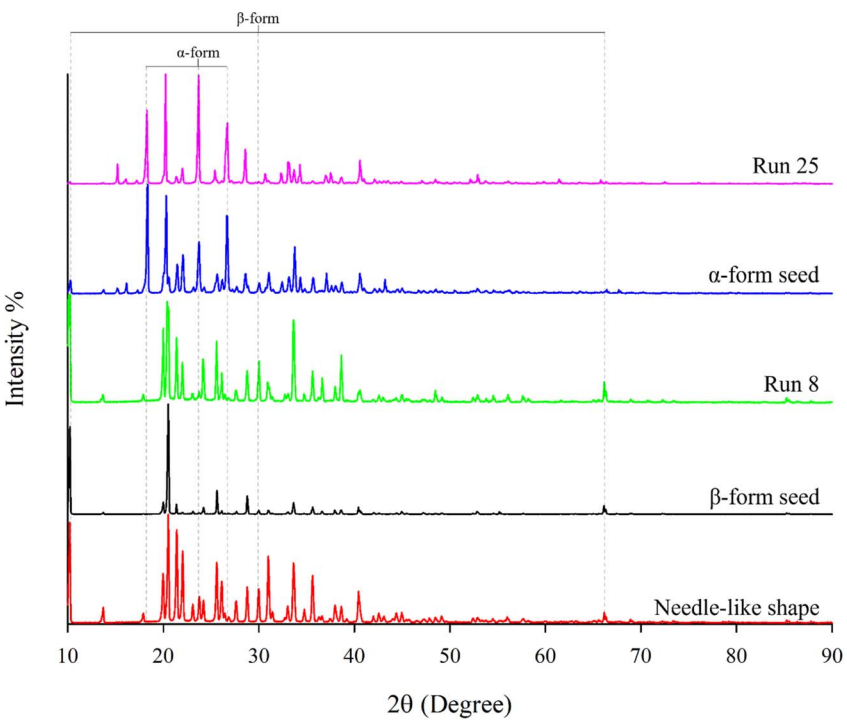

Fig. 7 XRD pattern – needle-like shape, β-form seed, Run 8, α-form seed, Run 25.

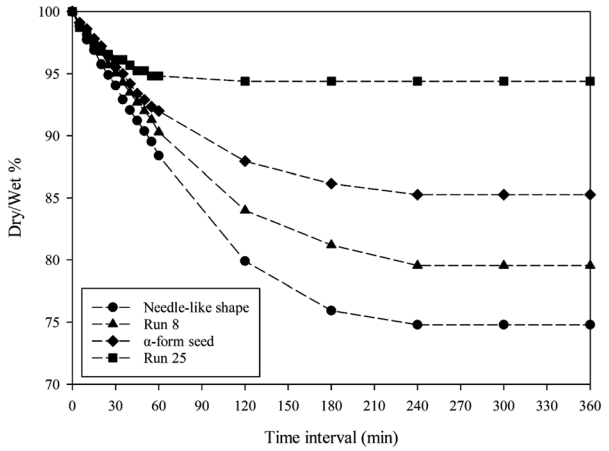

Fig. 8 Removal of mother liquor over time at room temperature.

After filtration, the needle-like shape and Run 25 exhibited different cake forms on the filter, as shown in Fig. 9. The mother liquor contents of the crystals appeared to vary depending on the cake structure formed.[43] The cake structure of the needle-like crystals appeared to be more compact than that of the crystals obtained in Run 25, which had a low aspect ratio. Needle-like crystals with a large aspect ratio, tend to cluster during filtration, potentially trapping the mother liquor or impurities between them.[44]

3.5 Aspect ratio and CSD

Fig. 10 and 11 show the aspect ratios and CSD of the crystals shown in needle-like shape, β-form seed, Run 8, α-form seed and 25, respectively. The aspect ratio is defined by eqn (4). The width and length of the crystal were measured across the center of the crystal, with the larger of the two values designated as "a". The crystal diameter was calculated using the following formula,[45] eqn (5):

$$\text{Aspect ratio(AR)} = \frac{a}{b} \tag{4}$$

$$\pi r^2 = L \times S \tag{5}$$

The needle-like shape crystals have a very high aspect ratio. Owing to seeding, the crystals obtained in Run 8 showed improvements in aspect ratio and average crystal diameter compared with those in β-form seed. Comparison of the crystals in α-form seed and Run 25 revealed that the average crystal diameter was larger in Run 25. The some crystals in Run 25 had higher aspect ratios than those in α-form seed, this is due to changes in the aspect ratio as the crystal grows. The overall average aspect ratio was lower in α-form seed. Nevertheless, the significant difference in mother liquor removal rate between these crystals (Fig. 8) suggest that the average crystal diameter (or size) has a stronger influence on the drying process than the crystal aspect ratio.

Fig. 9 OM image of a crystal being transferred to a Petri dish immediately after filtration, needle-like shape: looks like fiber, α-form seeded (Run 25): looks like grain of salt.

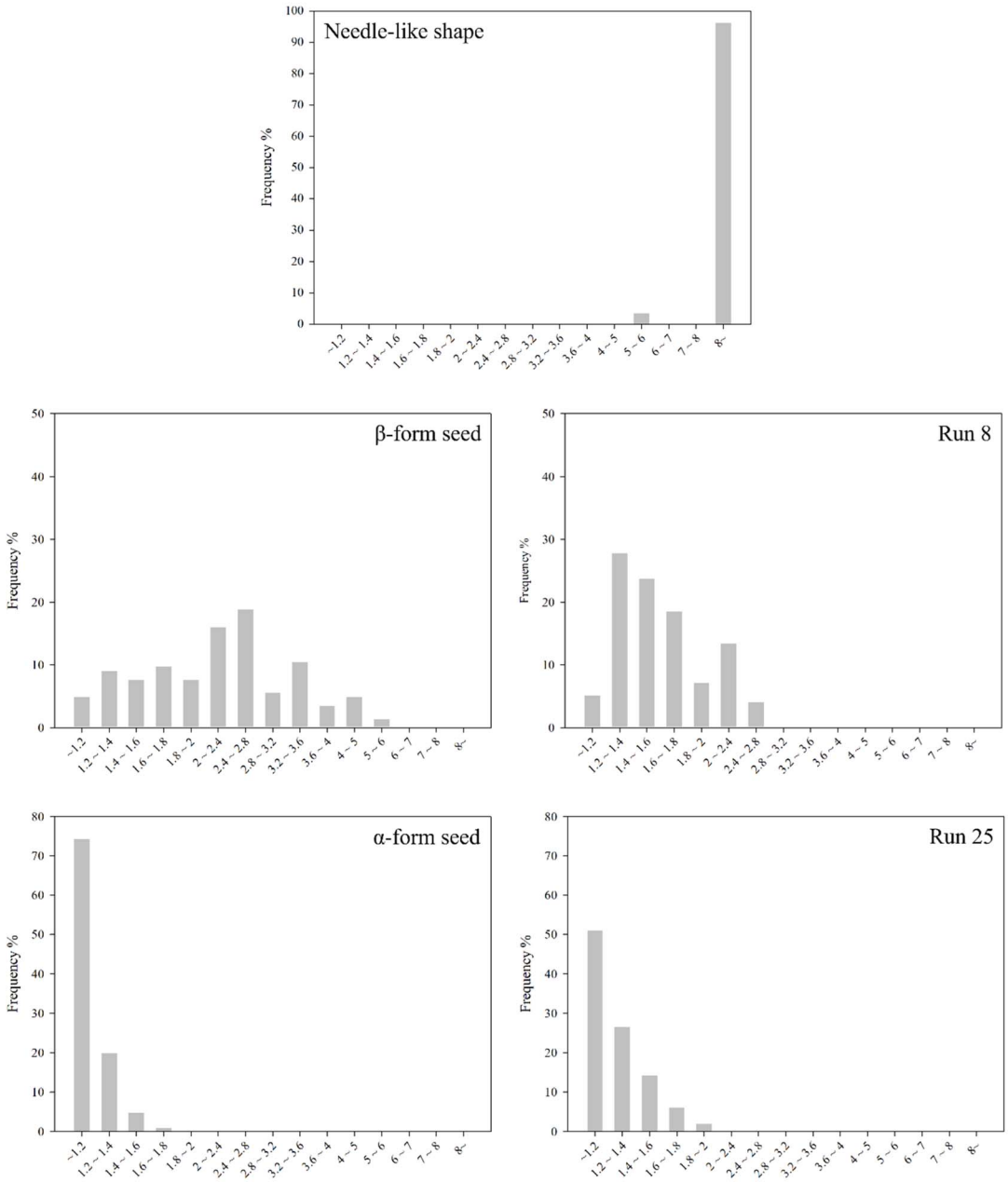

Fig. 10 Distribution of aspect ratio (*x*-axis: aspect ratio range).

Table 3 ranks the crystals based on the results shown in Fig. 8, 10 and 11. The most favorable crystals are characterized by a low aspect ratio (close to 1) and large diameter, corresponding to those in Run 25; these crystals have the lowest mother liquor content and fastest drying rate among the crystals investigated. Next, crystals with intermediate average crystal sizes (α-form seed and Run 8) were compared. Considering their mother liquor content and drying rate, α-form seed are preferable. Crystals with low aspect ratios are favored when the average crystal diameters in different cases are similar. Finally, the needle-like shape have the highest aspect ratio among the crystals considered and a relatively small diameter. The crystals obtained for this case also have a high mother liquor content and slow drying rate. Therefore, these crystals are considered the least preferred crystalline form. However, generalizing the results of this study to establish a 'preferred ranks the crystals' for LGA crystallization may be somewhat premature. Therefore, additional factors need to be considered for the crystallization target.

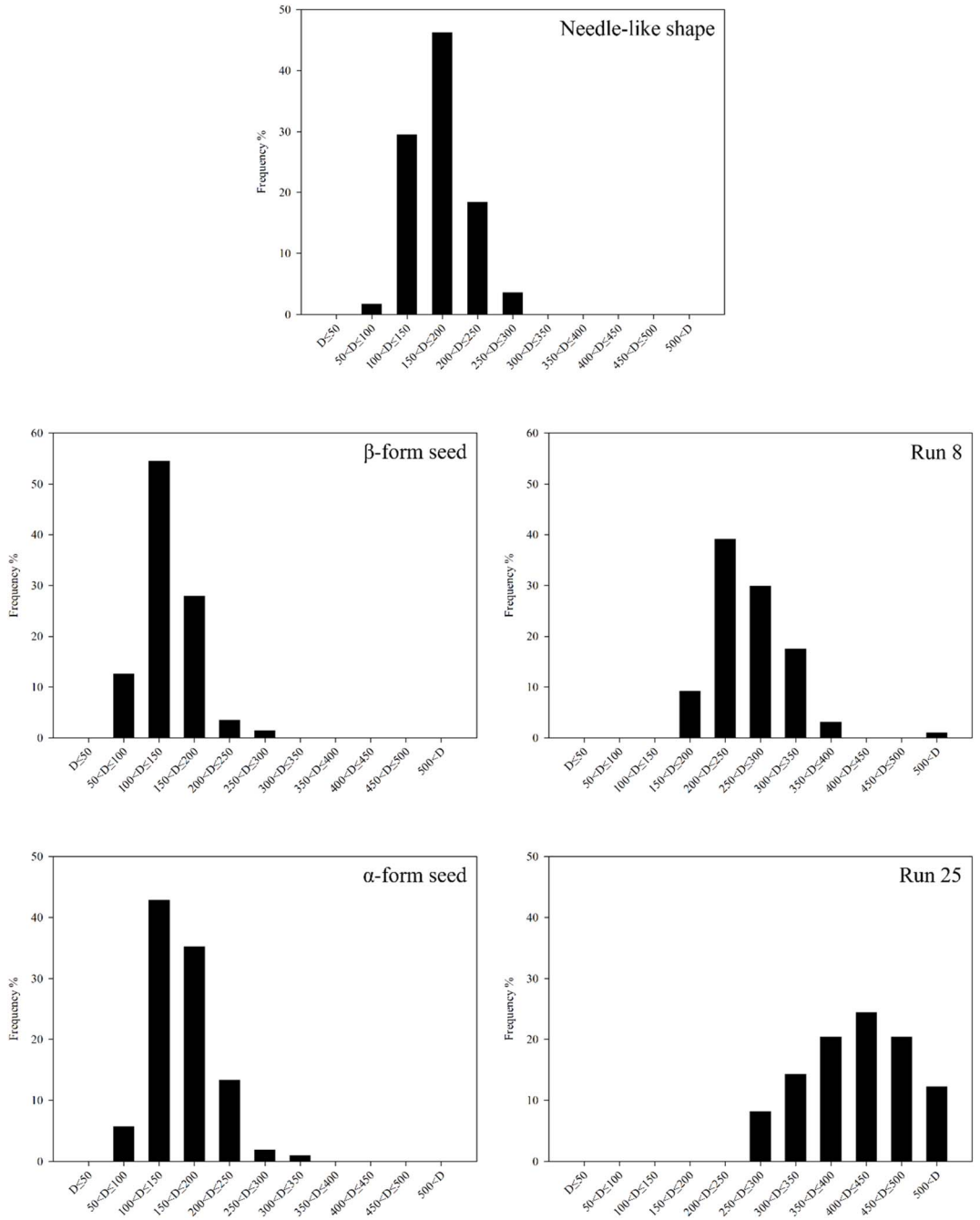

Fig. 11 Distribution of crystal diameter (*x*-axis: crystal diameter range).

Table 3 Preference rank based on aspect ratio, CSD, and drying efficiency in this study

Case	Crystalline form	Average crystal size	Mother liquor contents	Aspect ratio	Preference rank
Needle-like shape	β-Form	Small	High	High	4 (Bad)
Run 8	β-Form	Middle	Middle	Middle	3
α-Form seed	α-Form	Middle	Middle	Low	2
Run 25	α-Form	Large	Low	Low	1 (Good)

4. Conclusion

In the case of spontaneous nucleation, faster cooling rates lead to higher supersaturation, which favors the formation of isotropic α-form crystals. These results are consistent with those of previous studies. Seeding was used to improve the aspect ratio of the formed crystals. The α-form seeds showed improvements in aspect ratio under slow cooling rates and low supersaturation, whereas the β-form seeds showed improvements under fast cooling rates and high supersaturation. XRD analysis confirmed that the inherent crystalline form of the seed did not change, and that the crystals grew into a hexagonal shape when their aspect ratio was improved during seeding. The crystals obtained in Run 25 showed the greatest improvement in aspect ratio, lowest mother liquor content, and shortest drying time. However, drying was influenced not only by the aspect ratio, but also by the average crystal diameter. The results of this study indicate that a low aspect ratio and large average crystal diameter are optimal for the drying phase of the LGA crystallization process. The most favorable crystals were those grown using α-form seeds. If increasing the crystal diameter is not feasible, α-form seeds with a low aspect ratio obtained through spontaneous nucleation are the next best alternative for obtaining the desired crystals. However, a limitation of this study is the lack of detailed explanation regarding the crystal aggregation mechanism from a molecular perspective. Approaching the issue from a molecular perspective could provide deeper insights into the fundamental causes of aggregation beside the impact of crystal particle size and impact of aspect ratios.

Data availability

All data supporting the findings of this study are available from the corresponding author [J.-I. Park] on request.

Conflicts of interest

The authors declare that they have no known competing financial interests or personal relationships that could have appeared to influence the work reported in this paper.

Acknowledgements

This work was supported by Materials/Parts Technology Development Program (20020301, Development of waste carbon resource-based high-purity artificial graphite manufacturing technology for secondary battery anode material) funded by the Ministry of Trade, Industry & Energy (MOTIE, KOREA).

References

1 M. Kitamura, *J. Cryst. Growth*, 1989, **96**(3), 541–546.
2 K. Ramesh, D. Vikramachakravarthi and P. Pal, *Chem. Eng. Process.: Process Intensif.*, 2014, **81**, 59–71.
3 M. Chen, S. Du, T. Zhang, W. Qi, S. Wu and J. Gong, *Chem. Eng. Technol.*, 2018, **41**(6), 1259–1265.
4 S. Jiaa, Y. Gao, Z. Li, T. Zhang, J. Liua, J. Wang, Z. Gao and J. Gong, *Chem. Eng. Res. Des.*, 2022, **179**, 265–276.
5 S. Allan, *Myerson, Deniz Erdemir, Alfred Y. Lee*, Cambridge University Press, 2019.
6 C. Lindenberg and M. Mazzotti, *J. Cryst. Growth*, 2009, **311**(4), 1178–1184.
7 K. Srinivasan and P. Dhanasekaran, *J. Cryst. Growth*, 2011, **318**(1), 1080–1084.
8 Z. Gao, D. Zhu, Y. Wu, S. Rohani, J. Gong and J. Wang, *Cryst. Growth Des.*, 2017, **17**(10), 5007–5011.
9 Y. Ma, S. Wu, E. G. J. Macaringue, T. Zhang, J. Gong and J. Wang, *Org. Process Res. Dev.*, 2020, **24**(10), 1785–1801.
10 X. Ni and A. Liao, *Cryst. Growth Des.*, 2008, **8**(8), 2875–2881.
11 N. E. B. Briggs, U. Schacht, V. Raval, T. McGlone, J. Sefcik and A. J. Florence, *Org. Process Res. Dev.*, 2015, **19**(12), 1903–1911.
12 X.-W. Ni, A. Valentine, A. Liao, S. B. C. Sermage, G. B. Thomson and K. J. Roberts, *Cryst. Growth Des.*, 2004, **4**(6), 1129–1135.
13 A. Borissova, S. Khan, T. Mahmud, K. J. Roberts, J. Andrews, P. Dallin, Z.-P. Chen and J. Morris, *Cryst. Growth Des.*, 2009, **9**(2), 692–706.
14 E. S. Ferrari and R. J. Davey, *Cryst. Growth Des.*, 2004, **4**(5), 1061–1068.
15 T. Ono, J. H. ter Horst and P. J. Jansens, *Cryst. Growth Des.*, 2004, **4**(3), 465–469.
16 J. Scholl, D. Bonalumi, L. Vicum, M. Mazzotti and M. Muller, *Cryst. Growth Des.*, 2006, **6**(4), 881–891.
17 D. Mangin, F. Puel and S. Veesler, *Org. Process Res. Dev.*, 2009, **13**(6), 1241–1253.
18 C. Cashell, D. Corcoran and B. K. Hodnett, *J. Cryst. Growth*, 2004, **273**(1–2), 258–265.
19 C. Cashell, D. Sutton, D. Corcoran and B. Kieran Hodnett, *Cryst. Growth Des.*, 2003, **3**(6), 869–872.
20 C. Lindenberg, J. Scholl, L. Vicum, M. Mazzotti and J. Brozio, *Cryst. Growth Des.*, 2008, **8**(1), 224–237.
21 S. Liang, X. Duan, X. Zhang, G. Qian and X. Zhou, *Cryst. Growth Des.*, 2015, **15**(8), 3602–3608.
22 J. Bernstein, in *Polymorphism in Molecular Crystals*, Oxford Science Publications, 2nd edn, 2023.
23 T.-T. C. Lai, S. Ferguson, L. Palmer, B. L. Trout and A. S. Myerson, *Org. Process Res. Dev.*, 2014, **18**(11), 1382–1390.
24 Y. Tahri, E. Gagniere, E. Chabanon, T. Bounahmidi and D. Mangin, *J. Cryst. Growth*, 2016, **435**, 98–104.
25 Y. Sakata, *Agric. Biol. Chem.*, 1961, **26**(11), 355–361.
26 J. Orehek, D. Teslic and B. Likozar, *Org. Process Res. Dev.*, 2021, **25**(1), 16–42.
27 H. B. Matthews and J. B. Rawlings, *AIChE J.*, 2004, **44**(5), 1119–1127.
28 D. C. Huang, W. Liu, S. K. Zhao, Y. Q. Shi, Z. X. Wang and Y. M. Sun, *Chem. Eng. J.*, 2010, **156**(2), 360–365.
29 G. Fevotte and J. P. Klein, *Chem. Eng. J. Biochem. Eng. J.*, 1995, **59**(2), 143–152.
30 N. C. S. Kee, R. B. H. Tan and R. D. Braatz, *Cryst. Growth Des.*, 2009, **9**(7), 3044–3051.
31 E. Aamir, Z. K. Nagy and C. D. Rielly, *Chem. Eng. Sci.*, 2010, **65**(11), 3602–3614.

32 H. Takiyama, *Adv. Powder Technol.*, 2012, **23**(3), 273–278.
33 J. Aarthi, P. Dhanasekaran, T. S. Senthil and N. M. Ganesan, *J. Cryst. Growth*, 2018, **502**, 64–70.
34 F. Zhang, T. Liu, Y. Huo, R. Guan and X. Z. Wang, *J. Cryst. Growth*, 2017, **469**, 136–143.
35 T. Liu, Y. Cui, Y. Wang and Z. Kalman Nagy, *Ind. Eng. Chem. Res.*, 2022, **61**, 7.
36 T. D. Turner, N. Dawson, M. Edwards, J. H. Pickering, R. B. Hammond, R. Docherty and K. J. Roberts, *Cryst. Growth Des.*, 2022, **22**(5), 3042–3059.
37 A. Mersmann and K. Bartosch, *J. Cryst. Growth*, 1998, **183**(1–2), 240–250.
38 K.-J. Kim and A. Mersmann, *Chem. Eng. Sci.*, 2001, **56**(7), 2315–2324.
39 K.-J. Kim and M. F. Doherty, *AIChE J.*, 2015, **61**(4), 1372–1379.
40 E. M. Soper, R. Y. Penchev, S. M. Todd, F. Eckert and M. Meunier, *J. Cryst. Growth*, 2022, 591.
41 T. Thanh Huyen Trinha, C. Quang Khuu, S. E. Wolfa and A.-T. Nguyen, *J. Cryst. Growth*, 2020, 544.
42 S. Liang, X. Duan, X. Zhang, G. Qian and X. Zhou, *Cryst. Growth Des.*, 2015, **15**(8), 3547–4170.
43 R. Miyamoto, S. Amari and H. Takiyama, *J. Chem. Eng. Jpn.*, 2023, **56**, 1.
44 M. Lahav and L. Leiserowitz, *Chem. Eng. Sci.*, 2001, **56**(7), 2245–2253.
45 P. Kumar, D. Wilkinson and M. Li, *Particulate Systems Analysis*, 2006, **23**(2), 138–144.